Position Inverse Kinematics and Robust Internal-loop Compensator-based Control of a New Quadrotor Manipulation System

Ahmed Khalifa[1] **and Mohamed Fanni**[2]

[1,2]Department of Mechatronics and Robotics Engineering,
Egypt-Japan University of Science and Technology,
New Borg El-Arab City, Alexandria, Egypt
[2] On leave from Department of Production Engineering and Mechanical Design
Mansoura University, Mansoura, Egypt
ahmed.khalifa@ejust.edu.eg, mohamed.fanni@ejust.edu.eg

ABSTRACT

In this paper, the design and the position inverse kinematics analysis of a novel aerial manipulation system are presented. The proposed system consists of 2-link manipulator attached to the bottom of a quadrotor. This new system presents a solution for the limitations found in the current quadrotor manipulation system. New inverse kinematic analysis are derived such that quadrotor/joint space controller can be designed to track the required task space mission. To study the feasibility of the proposed system, a quadrotor with high enough payload to add the 2-link manipulator is designed and constructed. Experimental setup of the system is introduced and the design is verified experimentally. An experiment is carried out to estimate the rotors parameters. These parameters are used in the simulation and controller design of the proposed system in order to make more realistic setup. System dynamics are derived briefly based on Newton Euler Method. The controller of the proposed system is designed based on Robust Internal-loop Compensator (RIC) and compared to Fuzzy Model Reference Learning Control (FMRLC) technique which was previously designed and tested for the proposed system. These controllers are tested for provide system stability and trajectory tracking under the effect of picking as well as placing a payload and under the effect of changing the operating region. Simulation framework is implemented in MATLAB/SIMULINK environment with the real parameters. The simulation results indicate the feasibility and the efficiency the proposed inverse kinematic analysis and the proposed RIC-based control technique.

Keywords: Aerial Manipulation, Identification, Position Kinematic Analysis, Demining, Inspection, Transportation, Robust Internal-loop Compensator.

2010 Mathematics Subject Classification: 68T40, 70B10.

1 Introduction

Quadrotor is one of the Unmanned Aerial Vehicles (UAVs) which offer possibilities of speed and access to regions that are otherwise inaccessible to ground robotic vehicles. Quadrotor vehicles possess certain essential characteristics, such as small size and cost, Vertical

Take Off and Landing (VTOL), performing slow precise movements, and impressive maneuverability, which highlight their potential for use in vital applications. Such applications include; homeland security (e.g. Border patrol and surveillance), and earth sciences (to study climate change, glacier dynamics, and volcanic activity) (Gupte, Mohandas and Conrad, 2012), (Salih, Moghavvemi, Mohamed and Gaeid, 2010), (DiCesare, 2008), (Guo, Wang, Zheng and Wang, 2014), and (Kim, Kang and Park, 2010). However, most research on UAVs has typically been limited to monitoring and surveillance applications where the objectives are limited to "look" and "search" but "do not touch". Due to their superior mobility, much interest is given to utilize them for mobile manipulation such as inspection of hard-to-reach structures or transportation in remote areas. Previous research on aerial manipulation can be divided into three categories. The first approach is to install a gripper at the bottom of an UAV to hold a payload. In (Mellinger, Lindsey, Shomin and Kumar, 2011), (Lindsey, Mellinger and Kumar, 2012), and (Willmann, Augugliaro, Cadalbert, D'Andrea, Gramazio and Kohler, 2012), a quadrotor with a gripper is used for transporting blocks and to build structures. The second approach is to suspend a payload with cables. In (Bisgaard, la Cour-Harbo and Dimon Bendtsen, 2010), an adaptive controller is presented to avoid swing excitation of a payload. In (Michael, Fink and Kumar, 2011), specific attitude and position of a payload is achieved using cables connected to three quadrotors. The other types of research are concerned about interaction with existing structures, as example, for contact inspection. In (Torre, Mengoli, Naldi, Forte, Macchelli and Marconi, 2012) and (Albers, Trautmann, Howard, Nguyen, Frietsch and Sauter, 2010) research has been conducted on utilizing a force sensor or a brush as a manipulator. However, the above approaches have limitations for manipulation.

For the first category using a gripper, payloads are rigidly connected to the body of an UAV. Accordingly, not only the attitude of the payload is restricted to the attitude of the UAV, but also the accessible range of the end effector is confined because of the UAV body and blades. In the second type using cables, the movement of the payload cannot be always regulated directly because manipulation is achieved using a cable which cannot always drive the motion of the payload as desired. The last cases are applicable to specialized missions such as wall inspection or applying normal force to a surface.

To overcome these limitations, one alternative approach is to equip an aerial vehicle with a robotic manipulator that can actively interact with the environment. For example, in (Korpela, Danko and Oh, 2012), a test bed including four-DOF robot arms and a crane emulating an aerial robot is proposed. By combining the mobility of the aerial vehicle with the versatility of a robotic manipulator, the utility of mobile manipulation can be maximized. When employing the robotic manipulator, the dynamics of the robotic manipulator is highly coupled with of the aerial vehicle, which should be carefully considered in the controller design for the aerial vehicle. Also, an aerial robot needs to tolerate the reaction forces from the interactions with the object or external environment. These reaction forces may affect the stability of an aerial vehicle significantly.

In (Khalifa, Fanni, Ramadan and Abo-Ismail, 2012), we propose a new aerial manipulation system that consists of a 2-link manipulator attached to the bottom of a quadrotor. This new system presents a solution for the limitations found in the current quadrotor manipulation sys-

tem. It has the capability of manipulating the objects with arbitrary location and orientation (DOF are increased from 4 to 6), the manipulator provides sufficient distance between quadrotor and object location, and it is considered as the minimum manipulator weight for aerial manipulation. In (Khalifa, Fanni, Ramadan and Abo-Ismail, 2013), The dynamic model of this system is derived taking into account the effect of adding a payload to the manipulator, in addition to, the design of two controllers namely, Direct Fuzzy Logic controller and Fuzzy Model Reference Learning Control applied to this system, are presented. The simulation results indicate the outstanding performance of the FMRLC and the feasibility of the proposed robot. This proposed system opens new application area for robotics. Such applications are inspection, maintenance, firefighting, service robot in crowded cities to deliver light stuff such as post mails or quick meals, rescue operation, surveillance, demining, performing tasks in dangerous places, or transportation in remote places.
In (Orsag, Korpela and Oh, 2013), a quadrotor with light-weight manipulators are tested, although the movement of manipulator is not explicitly considered during the design of the PID controller. In (Kim, Choi and Kim, 2013), an aerial manipulation using a quadrotor with a 2 DOF robotic arm is presented but with different configuration from us. It did not provide a solution for the limited DOFs problem of aerial manipulation, in addition to, it did not provide explicit solution to the inverse kinematics problem.
In this paper the point-to-point kinematics analysis (forward and inverse) of the proposed system is derived. In addition, an experiment to identify rotors parameters is carried out. Moreover, controller design based on RIC is presented and compared on the previously designed FMRLC technique.
This paper is organized as following. Design of the proposed system is described in section 2. Section 3 introduces the system kinematic and dynamic analysis. The rotors parameters experiment is described in section 4. The proposed control system is presented in section 5. In section 6, simulation results using MATLAB/SIMULINK are presented. Finally, the main contributions are concluded in section 7.

2 Design of the Proposed System

The structure of the proposed system is shown in Fig. 1. The proposed quadrotor manipulation system consists mainly from two parts; the quadrotor and the manipulator.

2.1 Quadrotor

The quadrotor components are selected such that it can carry payload equals $500g$ (larger than the total arm weight and the maximum payload). Asctec pelican quadrotor (*Asctec Pelican Quadrotor*, 2014) is used as the quadrotor platform with the following specification: Autopilot sensor board, GPS receiver, Futuba R/C, X-bee, 11.1 V LiPo battery, 1.6 GHz Intel Atom processor board, and wireless LAN access point.

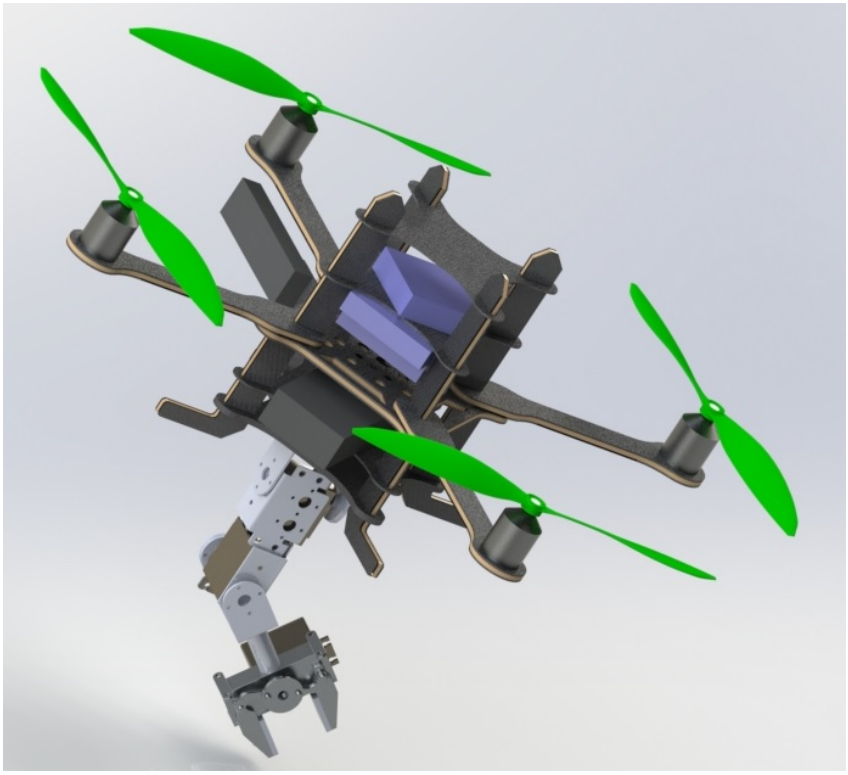

Figure 1: 3D CAD model of the New Quadrotor Manipulation System

2.2 The Two-Link Manipulator

Our target is to design a lightweight manipulator that can carry a payload of $200g$ and has maximum reach in the range between $22cm$ to $25cm$. The arm components are selected, purchased and assembled such that the total weight of the arm is $200g$ and can carry a payload of $200g$ (*Robotic Gripper for Robotic Arm*, 2014). The arm components are; Three DC motors (HS-422 (Max torque = $0.4N.m$) for gripper, HS-5485HB (Max torque = $0.7N.m$) for joint 1, and HS-422 (Max torque = $0.4N.m$) for joint 2), Motor's Driver (SSC-32) (Interface between the main control unit and the motors), Arduino board (Mega 2560) (*Arduino Board*, 2014) (Implement manipulator control algorithm), PS2 R/C (Remote controller to send commands to manipulator), and Motor accessories (Aluminum Tubing - $1.50in$ diameter, Aluminum Multi-Purpose Servo Bracket, Aluminum Tubing Connector Hub, and Aluminum Long "C" Servo Bracket with Ball Bearings) (*LYNXMOTION*, 2014).

The safety of this design and structure, with respect to the deflections and stress, is checked through finite element analysis using ANSYS software (see Figs. 2 and 3). From these figures, the maximum deflection is about 0.6 mm which is smaller than the allowable value which equals $1mm$. In addition, the maximum stress of the structure is $113MPa$ which is smaller than the yield strength of aluminum alloy which is $270MPa$. Also, the bearings and gripper are selected to carry the load Therefore, this design is safe.

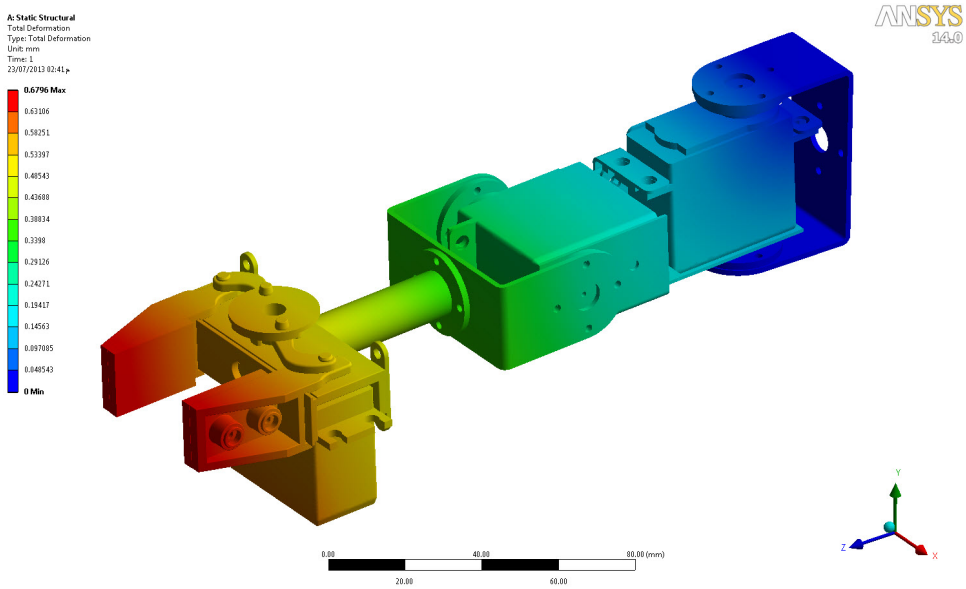

Figure 2: Manipulator's structure deflections using ANSYS

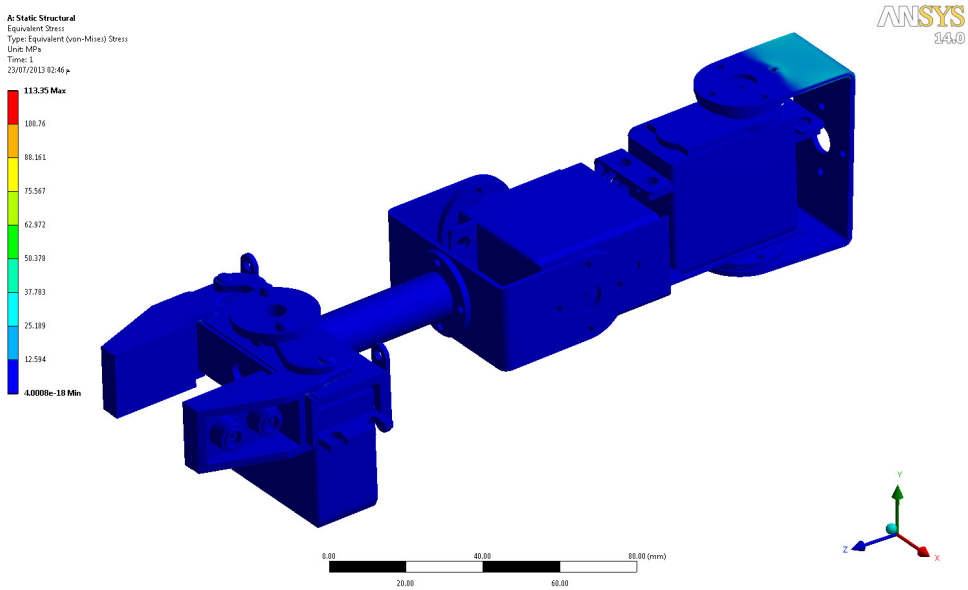

Figure 3: Manipulator's structure stress analysis using ANSYS

2.3 Validation

The whole system is connected as shown in Fig. 4. An experimental setup is carried out to validate the proposed design of the system. The experiment indicates the validity and safety of the design. The quadrotor can carry the manipulator with the target payload successfully. Position holding is one of the most important factors for accurate manipulation. The accurate measurements are crucial for using the aerial vehicle to manipulate an object as desired.
Fig. 5 shows the proposed experimental implementation of the whole connected system with the user interface and measurement system such that the position holding can be achieved. The ground station (PC, R/C, and Joystick) is used to monitor and send commands to system. The PC is connected to the on-board station (Atom Board) through WiFi network. The Atom

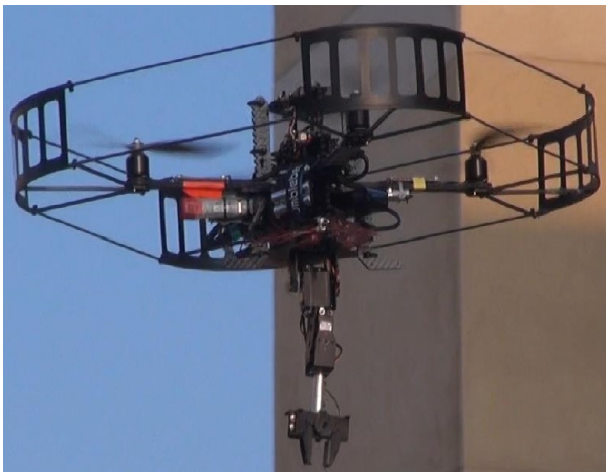

Figure 4: Experimental setup of the proposed system

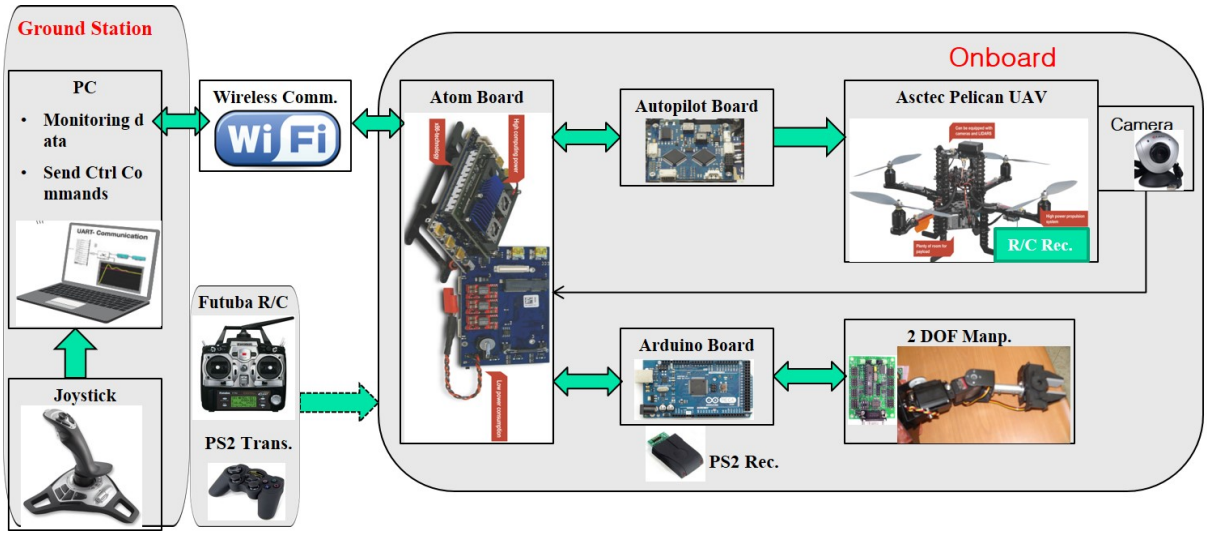

Figure 5: Aerial manipulation functional block diagram

Board, which runs under Linux platform, is used for control interface among ground PC, Arduino Board, and Autopilot Board. In addition, it is used to execute high computation algorithms, which is used for precise position estimation and control, such as VSLAM, Data fusion, and Planning. Moreover, the proposed architecture of the system enables it to operate in either autonomous or tele-operated mode.

3 Kinematics and Dynamics Analysis

Fig. 6 presents a sketch of the Quadrotor-Manipulator System with the relevant frames. The frames are assumed to satisfy the Denavit-Hartenberg (DH) convention (Leishman, 2000).
The manipulator has two revolute joints. The axis of the first revolute joint (z_0), that is fixed with respect to the quadrotor, is parallel to the body x-axis of the quadrotor (see Fig. 6). The axis of the second joint (z_1) will be parallel to the body y-axis of quadrotor at home (extended) configuration. Thus, the pitching and rolling rotation of the end effector is now possible independently on the horizontal motion of the quadrotor. Hence, With this new system, the capability of

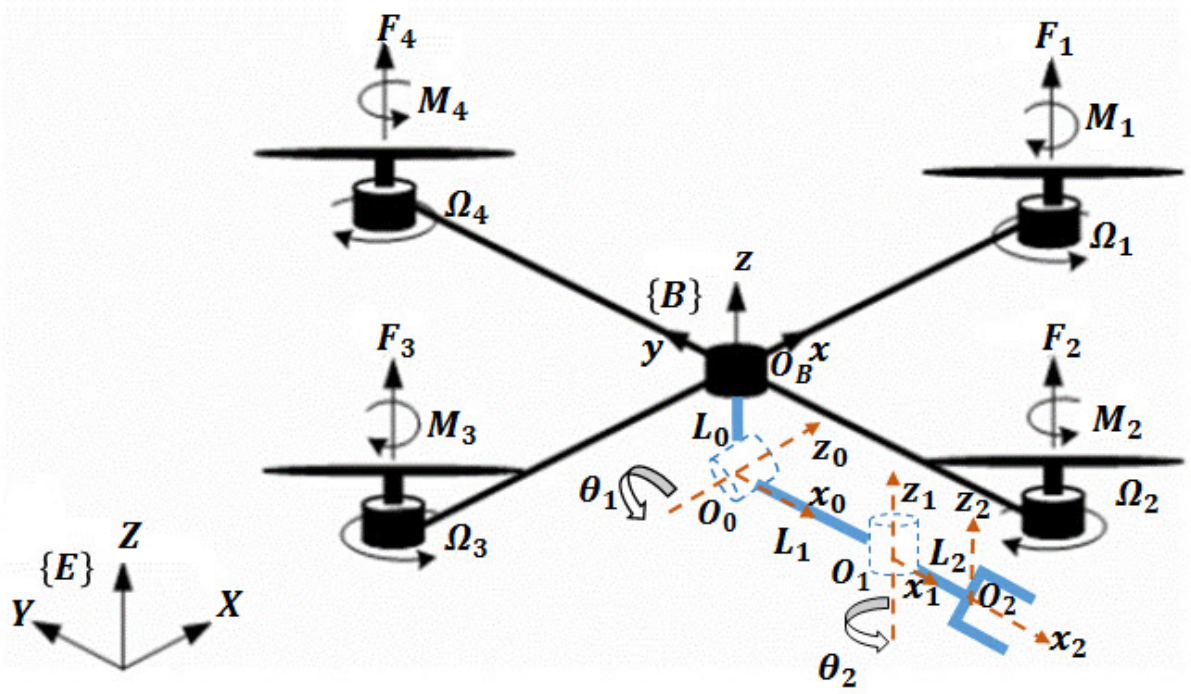

Figure 6: Schematic of Quadrotor Manipulation System Frames

manipulating objects with arbitrary location and orientation is achieved because the DOF are increased from 4 to 6.

3.1 Kinematics

The rotational kinematics of the quadrotor is represented through Euler angles. A rigid body is completely described by its position and orientation with respect to reference frame $\{E\}$, O_I-$X\ Y\ Z$, that it is supposed to be earth-fixed and inertial. Let define η_1 as

$$\eta_1 = [X, Y, Z]^T \tag{3.1}$$

the vector of the body position coordinates in the earth-fixed reference frame. The vector $\dot{\eta}_1$ is the corresponding time derivative. If one defines

$$\nu_1 = [u, v, w]^T \tag{3.2}$$

as the linear velocity of the origin of the body-fixed frame $\{B\}$, O_B-$x\ y\ z$, whose origin is coincident with the center of mass (CM), with respect to the origin of the earth-fixed frame expressed in the body-fixed frame, the following relation between the defined linear velocities holds:

$$\nu_1 = R_I^B \dot{\eta}_1 \tag{3.3}$$

where R_I^B is the rotation matrix expressing the transformation from the inertial frame to the body-fixed frame.
Let define η_2 as

$$\eta_2 = [\phi, \theta, \psi]^T \tag{3.4}$$

the vector of body Euler-angle coordinates in an earth-fixed reference frame. Those are commonly named roll, pitch and yaw angles and corresponds to the elementary rotation around X, Y and Z in fixed frame. The vector $\dot{\eta}_2$ is the corresponding time derivative (expressed in the inertial frame). Let define

$$\nu_2 = [p, q, r]^T \tag{3.5}$$

as body-fixed angular velocity. The vector $\dot{\eta}_2$ is related to the body-fixed angular velocity by a proper Jacobian matrix:

$$\nu_2 = J_v \dot{\eta}_2 \tag{3.6}$$

The matrix J_v can be expressed in terms of Euler angles as:

$$J_v = \begin{bmatrix} 1 & 0 & -S(\theta) \\ 0 & C(\phi) & C(\theta)S(\phi) \\ 0 & -S(\theta) & C(\theta)C(\phi) \end{bmatrix} \tag{3.7}$$

where $C(\alpha)$ and $S(\alpha)$ are short notations for $cos(\alpha)$ and $sin(\alpha)$. The rotation R_I^B matrix needed to transform the linear velocities, is expressed in terms of Euler angles by the following:

$$R_I^B = \begin{bmatrix} C(\psi)C(\theta) & S(\psi)C(\theta) & -S(\theta) \\ -S(\psi)C(\phi) + S(\psi)S(\theta)C(\psi) & C(\psi)C(\phi) + S(\psi)S(\theta)S(\phi) & C(\theta)S(\phi) \\ S(\psi)S(\phi) + C(\psi)S(\theta)C(\phi) & -C(\psi)S(\phi) + S(\psi)S(\theta)C(\phi) & C(\theta)C(\phi) \end{bmatrix} \tag{3.8}$$

The DH parameters for the 2-Link manipulator are derived and presented in (Khalifa et al., 2012).
The position and orientation of the end effector relative to the body-fixed frame is easily obtained by multiplying the following homogeneous transformation matrices A_0^B, A_1^0, A_2^1.

3.1.1 Forward Kinematics

Let define the position and orientation of the end effector expressed in the inertial frame, as η_{ee_1} and η_{ee_2} respectively.

$$\eta_{ee_1} = [x_{ee}, y_{ee}, z_{ee}]^T \tag{3.9}$$

$$\eta_{ee_2} = [\phi_{ee}, \theta_{ee}, \psi_{ee}]^T \tag{3.10}$$

The forward kinematics problem consists of determining the operational coordinates (η_{ee_1} and η_{ee_2}) of the end effector, as a function of the quadrotor movements (X, Y, Z, and ψ) as well as the motion of the manipulator's joints (θ_1 and θ_2). This problem is solved by computing the homogeneous transformation matrix composed of relative translations and rotations.
The transformation matrix from the body frame to the inertial frame A_B^I which is:

$$A_B^I = \begin{bmatrix} & & & X \\ & R_B^I & & Y \\ & & & Z \\ 0 & 0 & 0 & 1 \end{bmatrix}, \tag{3.11}$$

where R_B^I is $4x4$ matrix. The total transformation matrix that relates the end effector frame to the inertial frame is T_2^I, which is given by:

$$T_2^I = A_B^I A_0^B A_1^0 A_2^1 \tag{3.12}$$

Define the general form for this transformation matrix as a function of end effector variables(η_{ee_1} and η_{ee_2}), as following:

$$T_{ee} = \begin{bmatrix} r_{11} & r_{12} & r_{13} & x_{ee} \\ r_{21} & r_{22} & r_{23} & y_{ee} \\ r_{31} & r_{32} & r_{33} & z_{ee} \\ 0 & 0 & 0 & 1 \end{bmatrix} \tag{3.13}$$

Equating (3.12) and (3.13), an expression for the parameters of T_{ee} (r_{ij}, x_{ee}, y_{ee}, and z_{ee}; $i, j = 1, 2, 3$) can be found, from which values of the end effector variables can determined. Euler angles of the end effector (ϕ_{ee}, θ_{ee} and ψ_{ee}) can be computed from the rotation matrix of T_{ee} as in (Slabaugh, 1999).

3.1.2 Inverse Kinematics

The inverse kinematics problem consists of determining the quadrotor movements (X, Y, Z, and ψ) as well as the motion of the manipulator's joints (θ_1 and θ_2) as function of operational coordinates (η_{ee_1} and η_{ee_2}) of the end effector.

The inverse kinematics solution is essential for the robot's control, since it allows to compute the required quadrotor movements and manipulator joints angles to move the end effector to a desired position and orientation.

The rotations of the end effector can be parameterized by using several methods one of them, that is chosen, is the euler angles (Slabaugh, 1999).

Equation (3.12) can be expressed, after putting ϕ = θ = 0, since we apply for point-to-point control because we target end effector control during picking and placing positions (reset configuration), as following:

$$T_2^I = \begin{bmatrix} C(\psi)S(\theta_2) + C(\theta_1)C(\theta_2)S(\psi) & C(\psi)C(\theta_2) - C(\theta_1)S(\psi)S(\theta_2) & S(\psi)S(\theta_1) & X + L_1C(\theta_1)S(\psi) + L_2C(\psi)S(\theta_2) + L_2C(\theta_1)C(\theta_2)S(\psi) \\ S(\psi)S(\theta_2) - C(\psi)C(\theta_1)C(\theta_2) & C(\theta_2)S(\psi) + C(\psi)C(\theta_1)S(\theta_2) & -C(\psi)S(\theta_1) & Y - L_1C(\psi)C(\theta_1) + L_2S(\psi)S(\theta_2) - L_2C(\psi)C(\theta_1)C(\theta_2) \\ -C(\theta_2)S(\theta_1) & S(\theta_1)S(\theta_2) & C(\theta_1) & Z - L_0 - L_1S(\theta_1) - L_2C(\theta_2)S(\theta_1) \\ 0 & 0 & 0 & 1 \end{bmatrix} \tag{3.14}$$

From (3.14) and (3.13), the inverse kinematics of the system can be derived. According to the structure of (3.14), the inverse orientation is carried out first followed by inverse position. The inverse orientation has three cases as following:

CASE 1:

Suppose that not both of r_{13} , r_{23} are zero. Then from (3.14), we deduce that $sin(\theta_1) \neq 0$ and $r_{33} \neq \pm 1$. In the same time, $cos(\theta_1)$ = r_{33} and $sin(\theta_1)$ = $\pm\ \sqrt{1 - r_{33}^2}$ and thus,

$$\theta_1 = atan2(\sqrt{1 - r_{33}^2}, r_{33}) \tag{3.15}$$

or

$$\theta_1 = atan2(-\sqrt{1 - r_{33}^2}, r_{33}) \tag{3.16}$$

If we choose the value for θ_1 given by (3.15), then $sin(\theta_1) > 0$, and

$$\psi = atan2(r_{13}, -r_{23}) \tag{3.17}$$

$$\theta_2 = atan2(r_{32}, -r_{31}) \tag{3.18}$$

If we choose the value for θ_1 given by (3.16), then $sin(\theta_1) < 0$, and

$$\psi = atan2(-r_{13}, r_{23}) \tag{3.19}$$

$$\theta_2 = atan2(-r_{32}, r_{31}) \tag{3.20}$$

Thus, there are two solutions depending on the sign chosen for θ_1. If r_{13} = r_{23} = 0, then the fact that T_{ee} is orthogonal implies that r_{33} = $\pm$1.

CASE 2:

If r_{13} = r_{23} = 0 and r_{33} = 1, then $cos(\theta_1)$ = 1 and $sin(\theta_1)$ = 0, so that θ_1 = 0. In this case, the rotation matrix of (3.14)becomes

$$R_2^I = \begin{bmatrix} S(\theta_2+\psi) & C(\theta_2+\psi) & 0 \\ -C(\theta_2+\psi) & S(\theta_2+\psi) & 0 \\ 0 & 0 & 1 \end{bmatrix} \tag{3.21}$$

Thus the sum $\theta_2 + \psi$ can be determined as

$$\theta_2 + \psi = atan2(r_{11}, r_{12}) \tag{3.22}$$

We can assume any value for ψ and get θ_2. Therefor, there are infinity of solutions.

CASE 3:

If r_{13} = r_{23} = 0 and r_{33} = -1, then $cos(\theta_1)$ = -1 and $sin(\theta_1)$ = 0, so that θ_1 = π. In this case, the rotation matrix of (3.14) becomes:

$$R_2^I = \begin{bmatrix} S(\theta_2-\psi) & C(\theta_2-\psi) & 0 \\ C(\theta_2-\psi) & -S(\theta_2-\psi) & 0 \\ 0 & 0 & -1 \end{bmatrix} \tag{3.23}$$

Thus, $\theta_2 - \psi$ can be determined as

$$\theta_2 - \psi = atan2(r_{11}, r_{12}) \tag{3.24}$$

One can assume any value for ψ and get θ_2. Therefor, there are infinity of solutions.

In cases 2 and 3, putting ψ = 0 will lead to find θ_2.

Finally, the inverse position is determined from:

$$X = x_{ee} - (L_1C(\theta_1)S(\psi) + L_2C(\psi)S(\theta_2) + L_2C(\theta_1)C(\theta_2)S(\psi)) \tag{3.25}$$

$$Y = y_{ee} - (-L_1C(\psi)C(\theta_1) + L_2S(\psi)S(\theta_2) - L_2C(\psi)C(\theta_1)C(\theta_2)) \tag{3.26}$$

$$Z = z_{ee} - (-L_0 - L_1S(\theta_1) - L_2C(\theta_2)S(\theta_1)) \tag{3.27}$$

3.2 Dynamics

The equations of motion of the proposed robot are derived in details in (Khalifa et al., 2012). Applying Newton Euler algorithm (Tsai, 1999) to the manipulator considering that the link (with length L_0) that is fixed to the quadrotor is the base link, one can get the equations of motion of the manipulator as well as the interaction forces and moments between the manipulator and the quadrotor. The effect of adding a payload to the manipulator will appear in the parameters of its end link, link 2, (e.g. mass, center of gravity, and inertia matrix). Therefore, the payload will change the overall system dynamics.
The equations of motion of the manipulator are:

$$M_1\ddot{\theta_1} = T_{m_1} + N_1 \tag{3.28}$$

$$M_2\ddot{\theta_2} = T_{m_2} + N_2 \tag{3.29}$$

where, T_{m_1} and T_{m_2} are the manipulator actuators' torques. M_1, M_2, N_1, and N_2 are nonlinear terms and they are functions in the system states as described in (Khalifa et al., 2012).
The Newton Euler method are used to find the equations of motion of the quadrotor after adding the forces/moments from the manipulator are:

$$m\ddot{X} = T(C(\psi)S(\theta)C(\phi) + S(\psi)S(\phi)) + F^I_{m,q_x} \tag{3.30}$$

$$m\ddot{Y} = T(S(\psi)S(\theta)C(\phi) - C(\psi)S(\phi)) + F^I_{m,q_y} \tag{3.31}$$

$$m\ddot{Z} = -mg + TC(\theta)C(\phi) + F^I_{m,q_z} \tag{3.32}$$

$$I_x\ddot{\phi} = \dot{\theta}\dot{\phi}(I_y - I_z) - I_r\dot{\theta}\overline{\Omega} + T_{a_1} + M^B_{m,q_\phi} \tag{3.33}$$

$$I_y\ddot{\theta} = \dot{\psi}\dot{\phi}(I_z - I_x) + I_r\dot{\phi}\overline{\Omega} + T_{a_2} + M^B_{m,q_\theta} \tag{3.34}$$

$$I_z\ddot{\psi} = \dot{\theta}\dot{\phi}(I_x - I_y) + T_{a_3} + M^B_{m,q_\psi} \tag{3.35}$$

where F^I_{m,q_x}, F^I_{m,q_y}, and F^I_{m,q_z} are the interaction forces from the manipulator to the quadrotor in X,Y, and Z directions defined in the inertial frame and M^B_{m,q_ϕ} , M^B_{m,q_θ} , and M^B_{m,q_ψ} are the interaction moments from the manipulator to the quadrotor around X, Y, and Z directions defined in the body frame.
The variables in (3.30-3.35) are defined as follows: m is the mass of the quadrotor. Each rotor j has angular velocity Ω_j and it produces thrust force F_j and drag moment M_j which are given by:

$$F_j = K_{F_j}\Omega_j^2 \tag{3.36}$$

$$M_j = K_{M_j}\Omega_j^2 \tag{3.37}$$

where K_{F_j} and K_{M_j} are the thrust and drag coefficients.
T is the total thrust applied to the quadrotor from all four rotors, and is given by:

$$T = \sum_{j=1}^{4} (F_j) \tag{3.38}$$

T_{a_1}, T_{a_2}, and T_{a_3} are the three input moments about the three body axes, and are given as:

$$T_{a_1} = d(F_4 - F_2) \tag{3.39}$$

$$T_{a_2} = d(F_3 - F_1) \tag{3.40}$$

$$T_{a_3} = -M_1 + M_2 - M_3 + M_4 \tag{3.41}$$

d is the distance between the quadrotor center of mass and rotor rotational axis.

$$\overline{\Omega} = \Omega_1 - \Omega_2 + \Omega_3 - \Omega_4 \tag{3.42}$$

I_r is the rotor inertia. I_f is the inertia matrix of the vehicle around its body-frame assuming that the vehicle is symmetric about x-, y- and z-axis.

4 System Parameters Estimation

In order to test the feasibility of the proposed system, a simulation framework will be built. Thus, there is a need to find the real parameters of the system to make the simulation results more reliable. The identified parameters include the structure and rotor assembly parameters (K_{f_j} and K_{m_j}). To calculate the structure parameters, a 3D CAD model is developed using SOLIDWORKS software to calculate the mass moments of inertia and all the missing geometrical parameters. To estimate the rotor assembly parameters, an experimental setup of quadrotor is carried out, see Fig. 7. In this experiment, the rotor is mounted on a 6-DOF torque/force sensor that is connected to a NI Data Acquisition Card (NI DAC). Then, the DAC is connected to a PC running SIMULINK program as an interface to read data from DAC. The velocity of rotor is changed gradually and each time the generated thrust and drag moment is measured and recorded using SIMULINK program. By using MATLAB Curve Fitting toolbox the generated date are fitted by using (3.36 and 3.37), thus the thrust and moment coefficients can be obtained. The identified parameters are given in Table 1.

5 Controller Design

Quadrotor is an under-actuated system, because it has four inputs (angular velocities of its four rotors) and six variables to be controlled. By observing the operation of the quadrotor, one can find that the movement in X- direction is based on the pitch rotation, θ. Also the movement in Y- direction is based on the roll rotation, ϕ. Therefore, motion along X- and Y-axes will be controlled through controlling θ and ϕ.

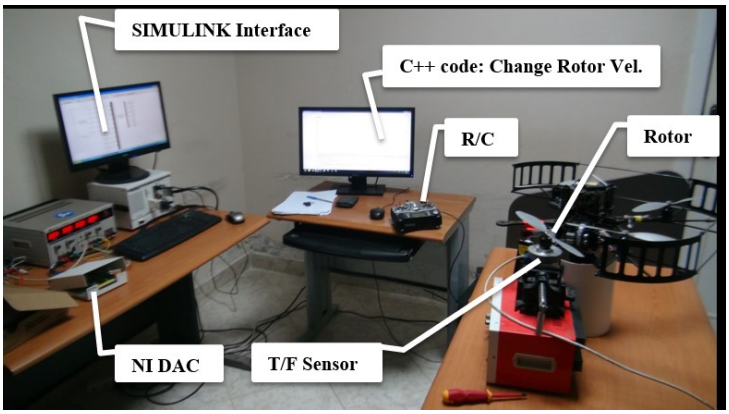

Figure 7: Experiment to estimate rotor coefficients

Table 1: System Parameters

Par.	Value	Unit	Par.	Value	Unit
m	1	kg	L_2	$85x10^{-3}$	m
d	$223.5X10^{-3}$	m	m_0	$30x10^{-3}$	kg
I_x	$13.215X10^{-3}$	$N.m.s^2$	m_1	$55x10^{-3}$	kg
I_y	$12.522X10^{-3}$	$N.m.s^2$	m_2	$112x10^{-3}$	kg
I_z	$23.527X10^{-3}$	$N.m.s^2$	I_r	$33.216X10^{-6}$	$N.m.s^2$
L_0	$30x10^{-3}$	m	L_1	$70x10^{-3}$	m
K_{F_1}	$1.667x10^{-5}$	$kg.m.rad^2$	K_{F_2}	$1.285x10^{-5}$	$kg.m.rad^2$
K_{F_3}	$1.711x10^{-5}$	$kg.m.rad^2$	K_{F_4}	$1.556x10^{-5}$	$kg.m.rad^2$
K_{M_1}	$3.965x10^{-7}$	$kg.m^2.rad^2$	K_{M_2}	$2.847x10^{-7}$	$kg.m^2.rad^2$
K_{M_3}	$4.404x10^{-7}$	$kg.m^2.rad^2$	K_{M_4}	$3.170x10^{-7}$	$kg.m^2.rad^2$

Fig. 8 presents a block diagram of the proposed control system. The desired values for the end effector's position (x_{ee_d}, y_{ee_d} and z_{ee_d}) and orientation (ϕ_{ee_d}, θ_{ee_d} and ψ_{ee_d}) are converted to the desired values of the quadrotor (X_d, Y_d, Z_d and ψ_d) and joints variables (θ_{1_d} and θ_{2_d}) through the inverse kinematics that are derived in section 3. Next, these values is applied to a trajectory generation algorithm which will be explained later. After that, the controller block receives the desired values and the feedback signals from the system and provides the control signals (T, τ_{a_1}, τ_{a_2}, τ_{a_3}, T_{m_1} and T_{m_2}). The matrix G of the control mixer, in Fig. 8, is used to transform the assigned thrust force and moments of the quadrotor (the control signals) from the controller block into assigned angular velocities of the four rotors. This matrix can be derived from (3.38-3.41) and presented as following:

$$\begin{bmatrix} \Omega_1^2 \\ \Omega_2^2 \\ \Omega_3^2 \\ \Omega_4^2 \end{bmatrix} = \underbrace{\begin{bmatrix} K_{F_1} & K_{F_2} & K_{F_3} & K_{F_4} \\ 0 & -dK_{F_2} & 0 & dK_{F_4} \\ -dK_{F_1} & 0 & dK_{F_3} & 0 \\ -K_{M_1} & K_{M_2} & -K_{M_3} & K_{M_4} \end{bmatrix}^{-1}}_{G} \begin{bmatrix} T \\ \tau_{a_1} \\ \tau_{a_2} \\ \tau_{a_3} \end{bmatrix} \tag{5.1}$$

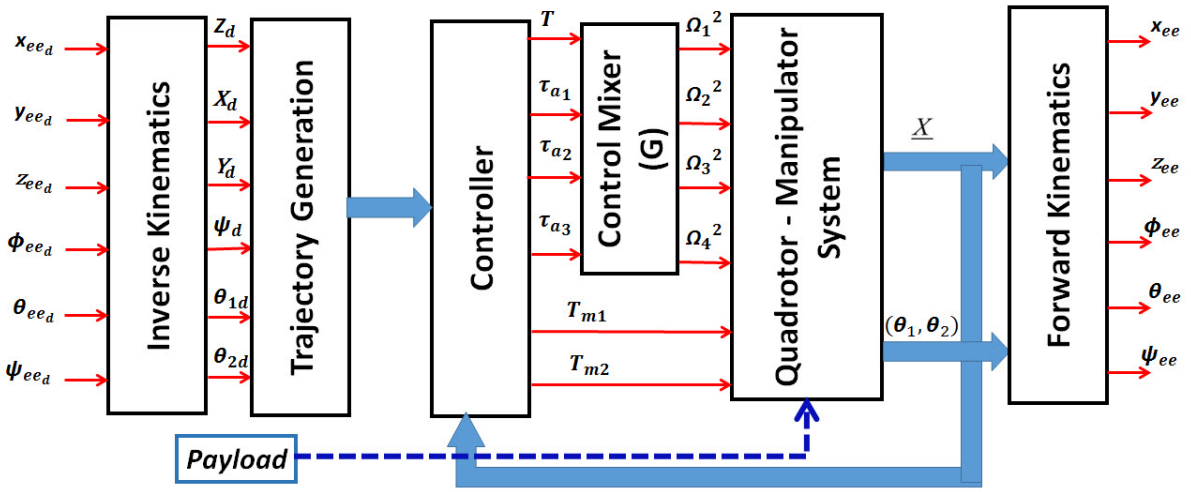

Figure 8: Block Diagram of the Control System

Finally, The actual values of the quadrotor and joints are converted to the actual values of the end effector variables through the forward kinematics which are derived in section 3.
The control design criteria are to achieve system stability and zero position error, for the movements in X, Y, Z, and ψ directions as well as for joints' angles θ_1 and θ_2 and consequently for the end effector variables (η_{ee_1} and η_{ee_2}), under the effect of:

- Picking and placing a payload.
- Changing the operating region of the system.

Noting that in the task space, a position tracking is implemented, and in the joint space, trajectory tracking is required.

5.1 Robust Internal-loop Compensator-based Control

Robust control is widely used in robotic system to ensure stability and robustness against external disturbances, uncertainties, and measurement noise (Hassanein, Anavatti and Ray, 2011). Disturbance Observer (DOb)-based controller design is one of the most popular methods in the field of motion control. In (Yamada, Komada, Ishida and Hori, 1996), the DOb-based controller is designed to realize a nominal system which can control acceleration in order to realize fast and precise servo system, even if servo system has parameter variation and suffers from disturbance. In (Kim and Chung, 2003) and (Kim, Choi, Lee and Koh, 2012), the generalized disturbance compensation framework, named the robust internal-loop compensator (RIC) is introduced and an advanced design method of a DOb is proposed based on the RIC. In (Park, Won, Kang, Kim, Lee and Kwon, 2005), the developed quadrotor shows stable flying performances under the adoption of RIC based disturbance compensation. Although a model is incorrect, RIC method can design a controller by regarding the inaccurate part of the model and sensor noises as disturbances.
We propose a robust internal loop compensator based control as robust controller to get accurate positioning of the proposed system. The controller consists of two parts, internal and

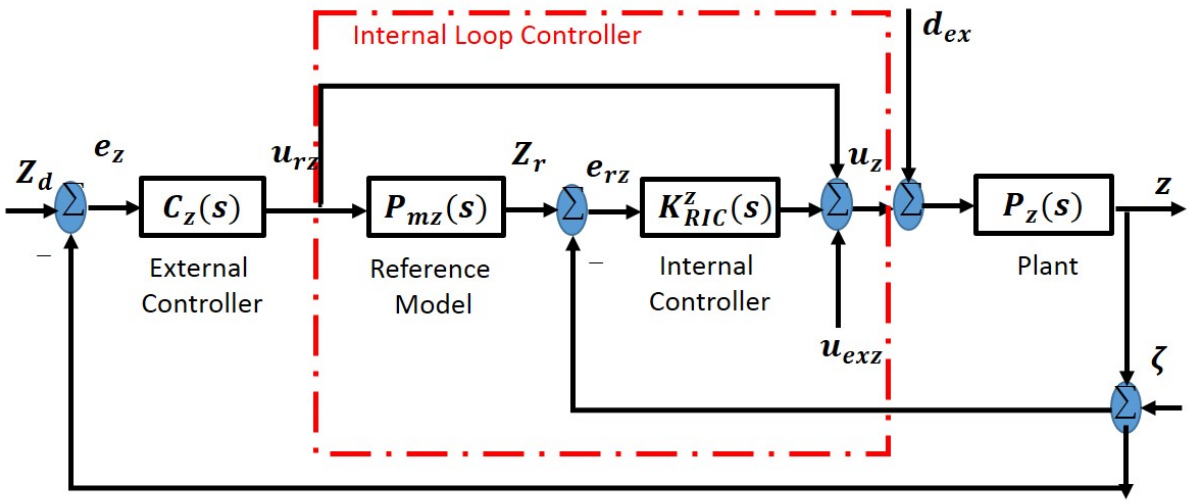

Figure 9: RIC Disturbance Compensation Controller

external loop. Internal loop is used as a compensator for canceling disturbances, uncertainties and nonlinearities including difference between reference model and real system, and external loop is designed to meet the specification of the system using the result of internal loop compensator.

The RIC based control algorithm, as shown in Fig. 9, controls the response of the plant $P(s)$ to follow that of the model plant $P_m(s)$ even though disturbances d_{ex} and sensor noise ζ are applied to the plant (Park et al., 2005). RIC based disturbance compensator can be used for position, attitude, and manipulator's joints control in the same way. For all controllers, the reference plant model are given in the form of:

$$P_{mi}(s) = \frac{1}{\tau_{c_i} s^2} \tag{5.2}$$

where $y_m(s)$ is the output response of the reference model (nominal plant), and $y_r(s)$ is the desired value of the plant. The value τ_i ($i = x$, y, z, ϕ, θ, ψ, θ_1, and θ_2), which depends on the plant dynamics, is mass for x, y, z-controller and mass moment of inertia for ϕ, θ, ψ, θ_1, and θ_2.

The external-loop compensator $C_z(s)$ for altitude (z) control, for instance, are given like PD controller as follows:

$$C_z(s) = k_{pz} + k_{dz} s \tag{5.3}$$

with the error e_z = z_r - z as the controller input. where k_{pz} and k_{dz} are P- and D-gain of the external-loop compensator, respectively. The output of the external-loop compensator, i.e., the reference input of RIC is given as

$$u_{rz}(s) = C_z(s) e_z \tag{5.4}$$

The output of the reference model is compared to the actual response generating the reference error e_{rz} = z_r - z which is applied to internal controller $K^z_{RIC}(s)$ that is chosen to be a PID-like controller and it is given as follows:

$$K^z_{RIC}(s) = k^z_p + k^z_d s + k^z_i \frac{1}{s} \tag{5.5}$$

Thus, the final control signal u_z is given as:

$$u_z = u_{cz} + u_{kz} + u_{exz} \tag{5.6}$$

where u_{cz} and u_{kz} are the control signals from the external and internal controllers respectively, while u_{exz} is an external value equal to the robot weight to compensate system weight (mg). The procedures for obtaining the RIC control input for X, Y, ϕ, θ, ψ, θ_1, and θ_2 control are the same with that for altitude (Z) control except that u_{exz} equal 0. In addition, there is difference in the design of X and Y controllers. In this control strategy, the desired pitch and roll angles, θ_d and ϕ_d , are not explicitly provided to the controller. Instead, they are continuously calculated by X and Y controllers in such a way that they stabilize the quadrotor's attitude. However, there is a need to convert the error and its rate of X and Y that is defined in the inertial frame into their corresponding values defined in the body frame. This conversion is done using the transformation matrix, defined in (3.8), assuming small angles (ϕ and θ) as following:

$$\tilde{x} = \tilde{X}\cos(\psi) + \tilde{Y}\sin(\psi) \tag{5.7}$$

$$\tilde{y} = \tilde{X}\sin(\psi) - \tilde{Y}\cos(\psi) \tag{5.8}$$

6 Simulation Results

Quintic Polynomial trajectories (Leishman, 2000) are used as the reference trajectories for X, Y, Z, ψ, θ_1, and θ_2. Those types of trajectories have sinusoidal acceleration which is better in order to avoid vibrational modes. The desired values of end effector position and orientation (Multi-region of operation and point-to-point control) are used to generate the desired trajectories for X, Y, Z, ϕ, θ and ψ using the inverse kinematics and then the algorithm for generating the trajectories.

The system equations of motion and the control laws for both FMRLC and RIC techniques are simulated using MATLAB/SIMULINK program. The design details, simulation results, and parameters of FMRLC can be found in (Khalifa et al., 2013).The controller parameters of the RIC controller are given in Table 2; we use the methodology for the RIC design given in (Kim and Chung, 2002) and the one used to design PID controllers in (Precup and Preitl, 2006). Those parameters are tuned to get the required system performance. The two controllers are tested to stabilize and track the desired trajectories under the effect of picking a payload of value 150 g at instant 15 s and placing it at instant 65 s. The simulation results of both FMRLC and RIC are presented in Fig. 10. These results show that RIC and FMRLC is able to track the desired trajectories (with different operating regions) before, during picking, holding, and placing the payload, in addition to, the RIC results is better than the FMRLC in disturbance rejection capability. Furthermore, the generated desired trajectories of θ and ϕ from RIC are smooth compared with that from FMRLC which are more oscillatory (see Fig. 10g and Fig. 10h). Moreover, since the RIC is simpler than FMRLC, the computation time for control laws of RIC is very small compared to that of FMRLC. Therefore, RIC is recommended to be implemented in experimental work.

Table 2: RIC Parameters

$Par./Val.$	X	Y	Z	ϕ	θ	ψ	θ_1	θ_2
k_{pi}	0.3	0.3	5	30	30	5	5	5
k_{di}	0.7	0.7	3	5	5	3	3	3
k_p^i	0.001	0.001	5	30	30	5	5	5
k_d^i	0.001	0.001	3	5	5	3	3	3
k_i^i	0	0	1	10	10	1	1	1
τ_{ci}	1	1	1	0.01	0.01	0.02	0.1	0.1

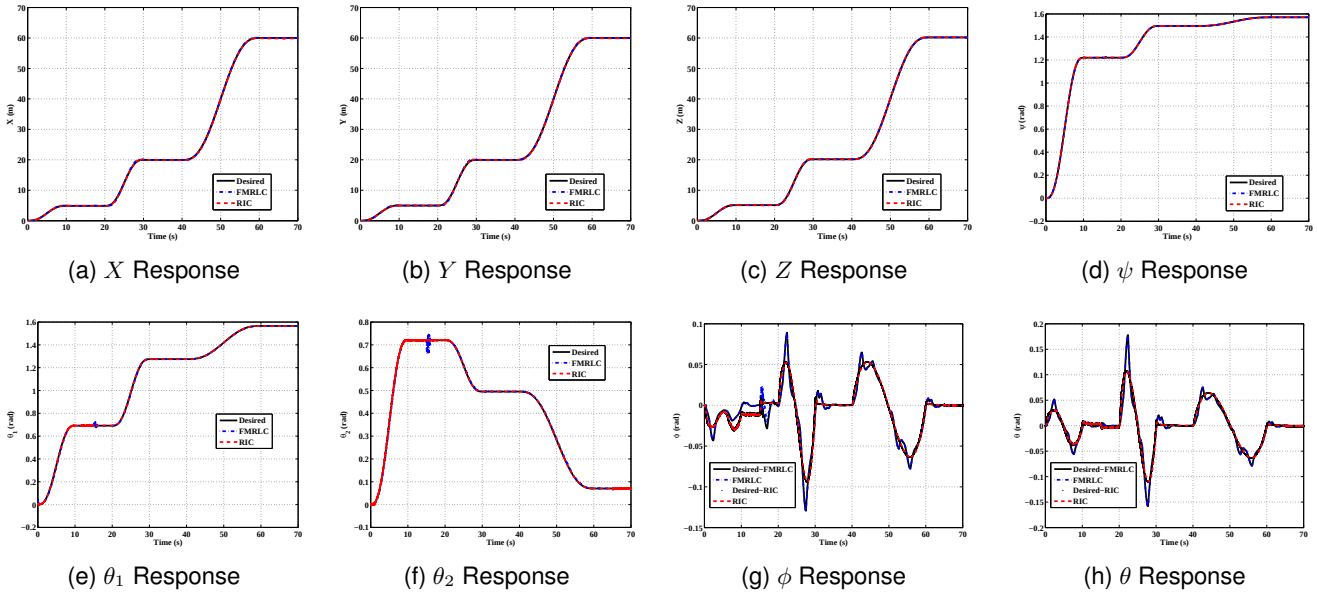

(a) X Response (b) Y Response (c) Z Response (d) ψ Response

(e) θ_1 Response (f) θ_2 Response (g) ϕ Response (h) θ Response

Figure 10: The Actual Response of RIC and FMRLC Techniques for the Quadrotor and Manipulator Variables: a) X, b) Y, c) Z, d) ψ, e) θ_1, f) θ_2, g) ϕ, and h) θ.

The end effector position and orientation can be found from the forward kinematics (see Fig. 11).

7 Conclusion

A new aerial manipulation robot is presented. Design and it experimental verification of this system is shown. Kinematic and Dynamic models of the proposed system are presented. Experimental setup of the proposed robot is shown and it is used with 6 DOF torque/force sensors to identify the rotor parameters. A new position inverse kinematics which is very simple compared to other trials in this direction is presented. RIC based control design is presented to control the proposed system and is compared to the FMRLC. These controllers are tested to provide system stability and trajectory tracking under the effect of picking and placing a payload and the effect of changing the operating region. The system equations of motion are simulated

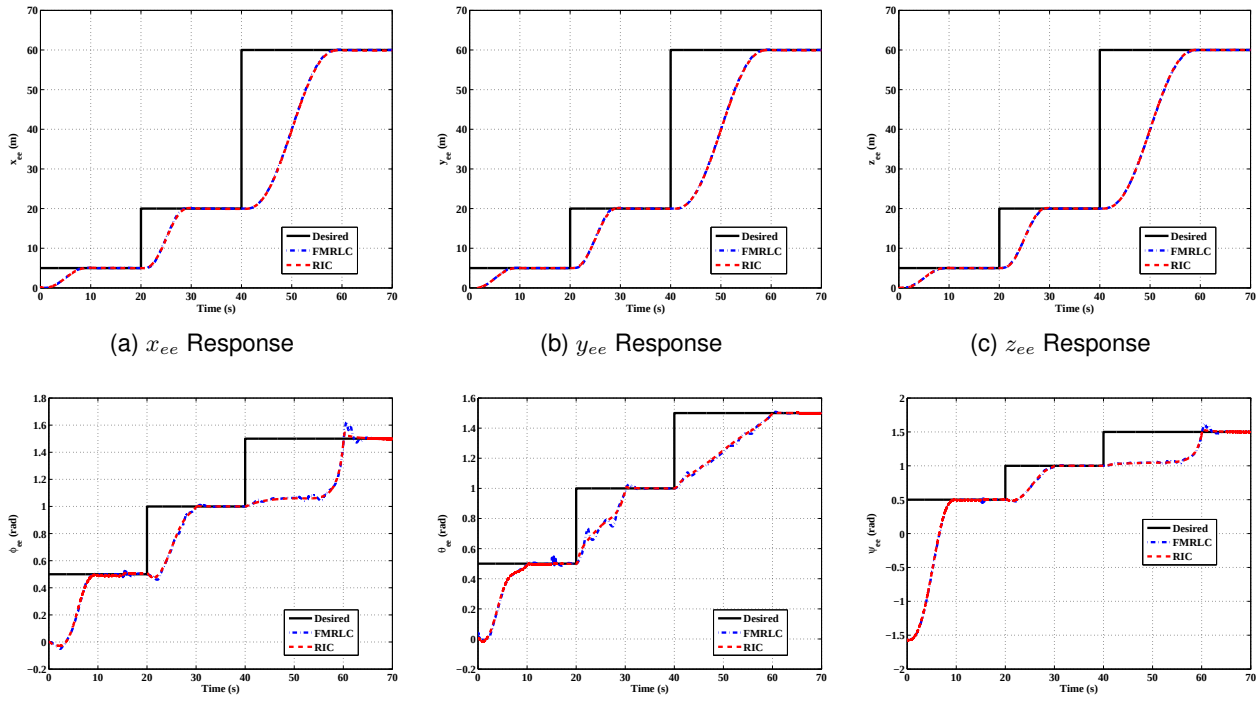

(a) x_{ee} Response (b) y_{ee} Response (c) z_{ee} Response

(d) ϕ_{ee} Response (e) θ_{ee} Response (f) ψ_{ee} Response

Figure 11: The Actual Response of both RIC and FMRLC Techniques for the End Effector Position and Orientation: a) x_{ee}, b) y_{ee}, c) z_{ee}, d) ϕ_{ee}, e) θ_{ee}, and f) ψ_{ee}.

using MATLAB/SIMULINK based on the system real parameters. Simulation results show that the RIC based control is very simple, has low computation time, and has higher disturbance rejection abilities comparing with FMRLC. In addition, these results indicate the feasibility of the proposed system. Therefore, the RIC is highly recommended to be implemented in real time to experimentally control the proposed system.

Acknowledgment

The first author is supported by a scholarship from the Mission Department, Ministry of Higher Education of the Government of Egypt which is gratefully acknowledged.

References

Albers, A., Trautmann, S., Howard, T., Nguyen, T. A., Frietsch, M. and Sauter, C. 2010. Semi-autonomous flying robot for physical interaction with environment, *Robotics Automation and Mechatronics (RAM), 2010 IEEE Conference on*, IEEE, pp. 441–446.

Arduino Board 2014. Available at `http://store.arduino.cc/product/A000067`.

Asctec Pelican Quadrotor 2014. Available at `http://www.asctec.de/en/uav-uas-drone-products/asctec-pelican/`.

Bisgaard, M., la Cour-Harbo, A. and Dimon Bendtsen, J. 2010. Adaptive control system for autonomous helicopter slung load operations, *Control Engineering Practice* **18**(7): 800–811.

DiCesare, A. 2008. *Design Optimization of a Quad-Rotor Capable of Autonomous Flight*, PhD thesis, WORCESTER POLYTECHNIC INSTITUTE.

Guo, J., Wang, Z., Zheng, M. and Wang, Y. 2014. An approach for uav reconnaissance mission planning problem under uncertain environment, *International Journal of Imaging and Robotics* **14**(3): 1–15.

Gupte, S., Mohandas, P. I. T. and Conrad, J. M. 2012. A survey of quadrotor unmanned aerial vehicles, *Southeastcon, 2012 Proceedings of IEEE*, IEEE, pp. 1–6.

Hassanein, O. I., Anavatti, S. G. and Ray, T. 2011. Robust position control for two-link manipulator, *International Journal of Artificial Intelligence* **7**(A11): 347–359.

Khalifa, A., Fanni, M., Ramadan, A. and Abo-Ismail, A. 2012. Modeling and control of a new quadrotor manipulation system, *2012 IEEE/RAS International Conference on Innovative Engineering Systems*, IEEE, pp. 109–114.

Khalifa, A., Fanni, M., Ramadan, A. and Abo-Ismail, A. 2013. Adaptive intelligent controller design for a new quadrotor manipulation system, *Systems, Man, and Cybernetics (SMC), 2013 IEEE International Conference on*, IEEE, pp. 1666–1671.

Kim, B. K. and Chung, W. K. 2002. Performance tuning of robust motion controllers for high-accuracy positioning systems, *Mechatronics, IEEE/ASME Transactions on* **7**(4): 500–514.

Kim, B. K. and Chung, W. K. 2003. Advanced disturbance observer design for mechanical positioning systems, *Industrial Electronics, IEEE Transactions on* **50**(6): 1207–1216.

Kim, J., Choi, S. B., Lee, H. and Koh, J. 2012. Design of a robust internal-loop compensator of clutch positioning systems, *Control Applications (CCA), 2012 IEEE International Conference on*, IEEE, pp. 1473–1478.

Kim, J., Kang, M.-S. and Park, S. 2010. Accurate modeling and robust hovering control for a quad-rotor vtol aircraft, *Selected papers from the 2nd International Symposium on UAVs, Reno, Nevada, USA June 8–10, 2009*, Springer, pp. 9–26.

Kim, S., Choi, S. and Kim, H. J. 2013. Aerial manipulation using a quadrotor with a two dof robotic arm, *Intelligent Robots and Systems (IROS), 2013 IEEE/RSJ International Conference on*, IEEE, pp. 4990–4995.

Korpela, C. M., Danko, T. W. and Oh, P. Y. 2012. Mm-uav: Mobile manipulating unmanned aerial vehicle, *Journal of Intelligent & Robotic Systems* **65**(1-4): 93–101.

Leishman, J. 2000. *Principles of Helicopter Aerodynamics*, Cambridge University Press.

Lindsey, Q., Mellinger, D. and Kumar, V. 2012. Construction with quadrotor teams, *Autonomous Robots* **33**(3): 323–336.

LYNXMOTION 2014. Available at `http://www.lynxmotion.com/default.aspx`.

Mellinger, D., Lindsey, Q., Shomin, M. and Kumar, V. 2011. Design, modeling, estimation and control for aerial grasping and manipulation, *2011 IEEE/RSJ International Conference on Intelligent Robots and Systems (IROS)*, IEEE, pp. 2668–2673.

Michael, N., Fink, J. and Kumar, V. 2011. Cooperative manipulation and transportation with aerial robots, *Autonomous Robots* **30**(1): 73–86.

Orsag, M., Korpela, C. and Oh, P. 2013. Modeling and control of mm-uav: Mobile manipulating unmanned aerial vehicle, *Journal of Intelligent & Robotic Systems* **69**(1-4): 227–240.

Park, S., Won, D., Kang, M., Kim, T., Lee, H. and Kwon, S. 2005. Ric (robust internal-loop compensator) based flight control of a quad-rotor type uav, *Intelligent Robots and Systems, 2005.(IROS 2005). 2005 IEEE/RSJ International Conference on*, IEEE, pp. 3542–3547.

Precup, R.-E. and Preitl, S. 2006. Pi and pid controllers tuning for integral-type servo systems to ensure robust stability and controller robustness, *Electrical Engineering* **88**(2): 149–156.

Robotic Gripper for Robotic Arm 2014. Available at `http://robokits.co.in`.

Salih, A. L., Moghavvemi, M., Mohamed, H. A. and Gaeid, K. S. 2010. Flight pid controller design for a uav quadrotor, *Scientific Research and Essays* **5**(23): 3660–3667.

Slabaugh, G. G. 1999. Computing euler angles from a rotation matrix, *Retrieved on August* **6**: 2000.

Torre, A., Mengoli, D., Naldi, R., Forte, F., Macchelli, A. and Marconi, L. 2012. A prototype of aerial manipulator, *Intelligent Robots and Systems (IROS), 2012 IEEE/RSJ International Conference on*, IEEE, pp. 2653–2654.

Tsai, L.-W. 1999. *Robot analysis: the mechanics of serial and parallel manipulators*, Wiley-Interscience.

Willmann, J., Augugliaro, F., Cadalbert, T., D'Andrea, R., Gramazio, F. and Kohler, M. 2012. Aerial robotic construction towards a new field of architectural research, *International journal of architectural computing* **10**(3): 439–460.

Yamada, K., Komada, S., Ishida, M. and Hori, T. 1996. Analysis of servo system realized by disturbance observer, *Advanced Motion Control, 1996. AMC'96-MIE. Proceedings., 1996 4th International Workshop on*, Vol. 1, IEEE, pp. 338–343.